Iranian Journal of Materials Forming 8 (1) (2021) 26-38

Online ISSN: 2383-0042

Iranian Journal of Materials Forming

Journal Homepage: http://ijmf.shirazu.ac.ir

Research Article

Developing the Cu/Sn Multilayer Composite through Accumulative Roll Bonding (ARB): Investigating the Microstructural and Mechanical Features

M. Javanmardi[1] and L. Ghalandari[*2]

[1] Department of Mechanical Engineering, Islamic Azad University, Shiraz Branch, Shiraz, Iran
[2] Department of Materials Science and Engineering, Islamic Azad University, Shiraz Branch, Shiraz, Iran

ARTICLE INFO

Article history:

Received 11 August 2020
Reviewed 13 September 2020
Revised 1 November 2020
Accepted 4 November 2020

Keywords:

Cu/Sn composites
Multilayer
Accumulative roll bonding
SPD
FESEM
XRD
Fractography
Grain-refinement

ABSTRACT

In this research, multilayer Cu/Sn composites were produced for the first time with the accumulative roll bonding (ARB) method using the commercial pure Cu and Sn sheets in up to eight cycles. The microstructural and mechanical properties of the Cu/Sn composites were studied during various ARB cycles by field emission scanning electron microscopy (FESEM), elemental mapsand X- ray diffraction (XRD), as well as tensile and Vickers micro-hardness tests. The results revealed that the necking and rupturing of the layers take place after 2 and 3 cycles, respectively. The final microstructure consists of the uniform distribution of the hard copper fragments and wavy soft Sn matrix. XRD and FESEM results confirmed the formation of the intermetallic Cu_6Sn_5 compound after 6 cycles. The maximum tensile strength reached 290 MPa after one ARB cycle, which is around 1.4 and 13 times higher than that of the pure Cu and Sn, respectively; thereafter, it decreased and then increased up to 150 MPa in the 8th cycle. The hardness of the copper layers increased by rising the number of ARB cycles. The tensile fracture mode for Cu and Sn layers was ductile in all ARB cycles. Further dimples were observed in the copper layers.

1. Introduction

In the last two decades, numerous multilayers have been produced by the accumulative roll bonding (ARB), which is one of the severe plastic deformation (SPD) methods for producing bulk nanostructure materials. This method is similar to the other SPD methods in regard to producing the ultrafine-grain structure with high strength without any change in the initial sample dimensions. At the first step of this method, the degreased and wire-brushed sheets are stacked on each other and then the layers are rolled, repeatedly [1]. The method was first developed by Saito et al. [1] and performed on pure metals such as Al [1, 2], Cu [3] and Ti [4], as well as on alloy systems like Al, copper and magnesium alloys, etc. [5-9]. Besides its basic applications for the production of the UFG materials, the ARB has recently been used as an effective tool for the fabrication of the particulate metal matrix composites [10-15] and multi-layered composite materials [16-22].

Through this method, multilayered composites with layers of extra thin thickness have been produced [16, 23-31]. In some two- or three-layer metallic composites produced by this method, the strength has been two or three times that of the initial layers [17, 20, 26, 30]. The main reasons for increasing the strength are grain refinement and strain hardening [20, 31]. However, in a

* Corresponding author
E-mail address: lgh@iaushiraz.net (L. Ghalandari)
https://doi.org/10.22099/ijmf.2020.38097.1165

few systems the strength is reduced for some reasons. In some of them the reasons are the dynamic recovery or recrystallization of the softer layers [18, 19, 32] while in others, it is the creation of defects like voids, porosities, cracks, etc. [16, 17, 33] and the intermetallic compounds [31].

In our previous studies we had observed the Kirkendall porosity in Cu/Zn [16] and Cu/Zn/Al [17] systems, which is another reason for decreasing the strength. The reason for creating the porosities is the difference in the melting point of the two adjacent layers, which leads to some difference in the diffusion rate of the elements at the interface between the layers [17].

Now, we intend to examine the probability of creating these porosities in other laminated composites like copper and tin, which differ noticeably in their melting temperature.

Cu-Sn alloys and their composites are being widely used in sliding bearings and bushes in automotive applications due to good bearing and wear properties, as well as their lower cost. In order to improve the wear characteristics, the composite materials must have a phase/reinforcement capable of providing thermal stability, as well as strengthening and lubricating the properties [34, 35]. The ARB method has a good capability in producing multilayer composites with high strength, ultra-fine grains and ultra-thin sub-layers. Accordingly, we examined the possibility of the Cu/Sn multilayer composite fabrication via this method. After that the structural and mechanical properties of the produced multilayered composites were investigated.

2. Material and Methods

In this study the utilized materials included two kinds of metal sheet, including commercial pure 50 mm × 100 mm annealed copper and tin strips with the given composition in Table 1 and the thickness of 0.9 and 0.5 mm, respectively. The multilayer composites were made in two stages: First, a primary sandwich was prepared using two Cu sheets and one Sn sheet in the middle.

To achieve the initial appropriate bonding, in the first cycle (namely zero cycle) the initial sandwich was cold rolled by a 57% reduction in thickness. In the next stage (ARB), the sandwich was cut into two halves and fastened by copper wires at the four corner points in order to avoid sliding onto each other. The roll bonding was performed by a reduction in the thickness of 50%. The process was conducted at room temperature and repeated in up to 8 cycles without lubrication. In the two stages prior to putting the metal sheets and composite layers on each other, they were degreased by acetone and wire brushed by a circular steel brush. The rolling process was carried out at room temperature by a 170 mm roll (in diameter) at a 20 rpm rolling speed with a loading capacity of 20 tons. The cross-section of the multilayer composites was examined on the normal direction-rolling direction (ND-RD) sections by a field emission scanning electron microscope (FESEM). The X-ray diffraction (XRD) analysis was conducted to identify the present phases in the microstructure by a diffractometer operating at 40 kV and 30 mA with Cu Kα radiations and step time of 4s.

The tensile samples were machined from the ARB-processed strips according to the 1/2 subsize specimen based on the ASTM E8/E8M 16a standard with orientation along the rolling direction. The gauge width and length of the samples were 3 and 15 mm, respectively. The tensile tests were done at room temperature by a tensile testing machine with a nominal initial strain rate of 10^{-4} s^{-1}. For each cycle, 3 tensile samples were prepared and tested, and the average results were reported. The Vickers hardness test was done on Cu and Sn layers, separately, at more than five points, using the Koopa apparatus under a load of 10 g for 15 s.

Table 1. The chemical composition (wt. %) of the materials used in this study

Cu (99.4)														
Zn	Pb	Sn	P	Mg	Fe	Ni	Si	Ag	Co	Mg	Cr	Al	S	As
<0.005	0.029	<0.005	0.003	0.007	<0.005	<0.005	<0.005	0.008	0.013	0.002	0.002	0.002	<0.002	0.004
Sn>99.7														
				Pb	Cu	Bi	Fe	Al	Zn	Sb				
				0.04	0.02	0.02	0.01	0.01	<0.01	<0.01				

3. Results and Discussion

3.1 Microstructure evolution

Figure 1 shows the FESEM micrographs of the microstructure of the Cu/Sn multilayers, parallel to the RD-ND plane after various ARB cycles.

As can be seen, this multilayer composite system resembles the previous systems [16-18, 23] in regard to decreasing the thickness of the layers and increasing the number of layers per unit thickness. Moreover, in the early stages, the interface between the layers is straight. In the intermediate cycles (after two cycles), some irregularities occur at the interface, causing them to become wavy. At the last stages the lenticular fragments in the microstructure resulting from rupturing along the necked regions can be observed. Additionally, there are no cracks or pores at the interface of the layers, which is why the bonding of the Cu and Sn layers is suitable.

In the following figures and discussions, the microstructure evolution has been described in more detail. The FESEM image, accompanied by the elemental distribution maps after two ARB cycles, has been shown in Fig. 2. At this stage, Cu starts to neck as a hard phase with respect to Sn, confirming the results of some other reports [16, 19]. Based upon these reports, it has been concluded that the onset of the instability of the layers depends upon their thickness difference and mechanical properties, regardless of their crystal structures [18]. The mechanical properties of the copper and tin layer have been depicted in Table 2.

As can be seen, the tensile strength and hardness of the copper layer are higher than that of the tin layer. Hence, it necks earlier than the Sn layer [18].

Figure 3 shows the image with the elemental distribution maps after the third cycle. As can be seen, due to the high strain arising from the rolling pressure, the two Sn layers reach each other and cause a severe necking in the copper layer; moreover, a partial necking is observed in the tin layers. In this condition, the rupturing of the copper layers takes place. This has been indicated by arrows in the figure. The FESEM image with elemental distribution maps after four ARB cycles has been depicted in Fig. 4.

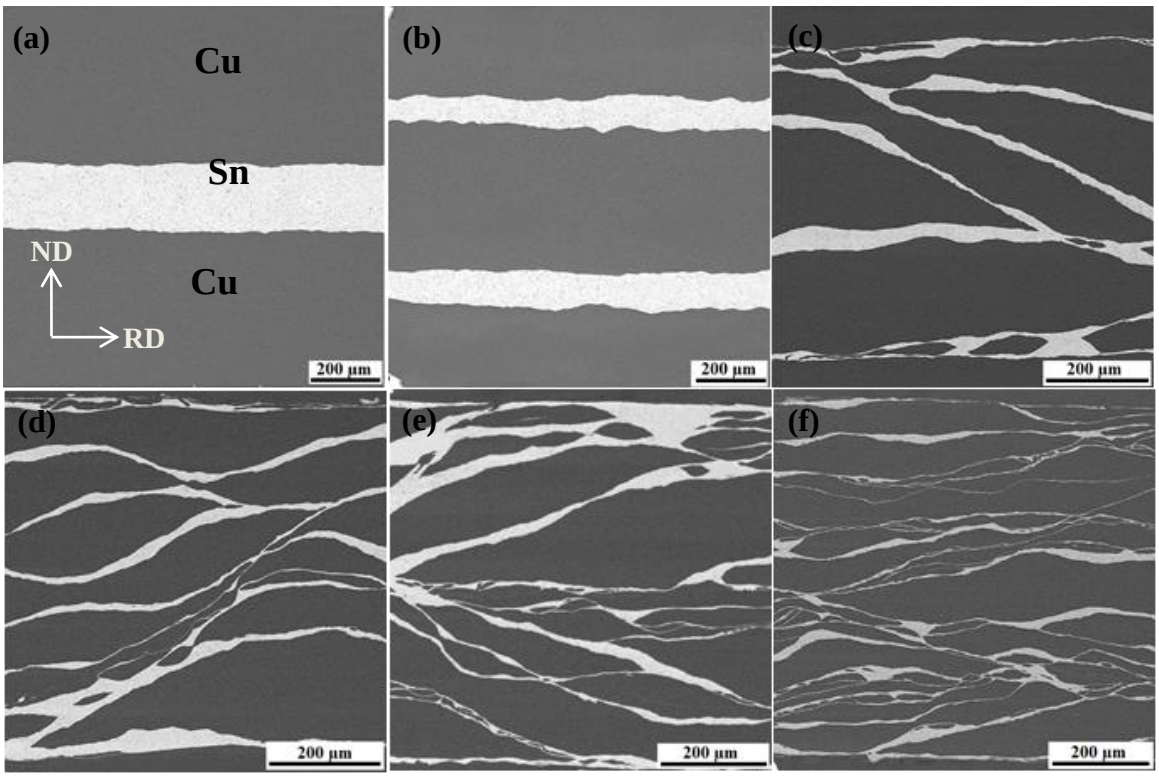

Fig. 1. FESEM micrographs of the ARB-processed Cu/Sn composites after: (a) zero, (b) one, (c) three, (d) five, (e) six and (f) seven cycles; the bright areas are related to the tin.

Table 2. The mechanical properties of the pure and annealed Cu and Sn

Element	Strain hardening exponent	Coefficient of strength (MPa)	Tensile strength (MPa)	Hardness (Hv)	Melting temperature (°C)
Cu	0.478	459.4	202	54	1084.62
Sn	0.31	44.37	22	8	231.9

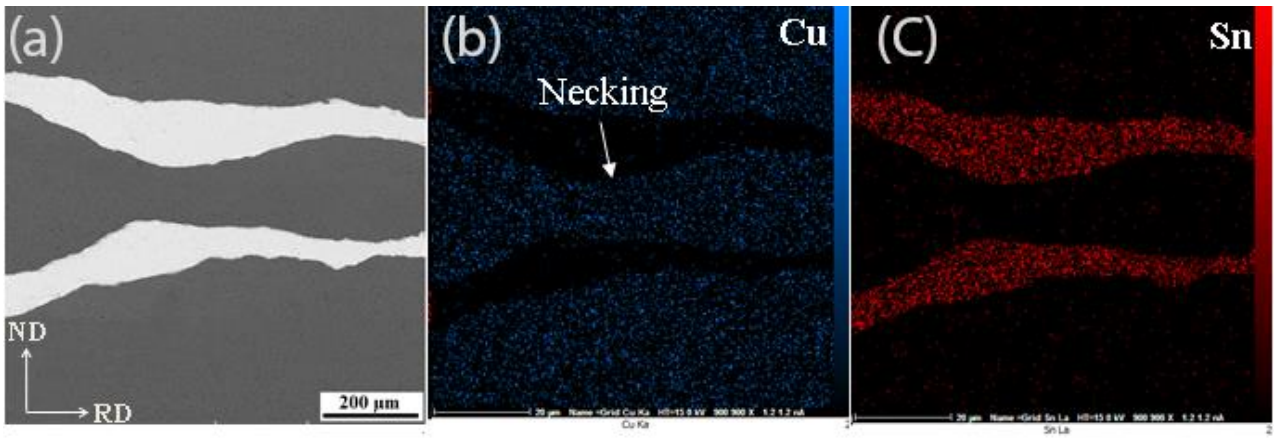

Fig. 2. (a) FESEM image of the Cu/Sn composite after two cycles and the corresponding FESEM elemental maps for (b) Cu distribution and (c) Sn distribution.

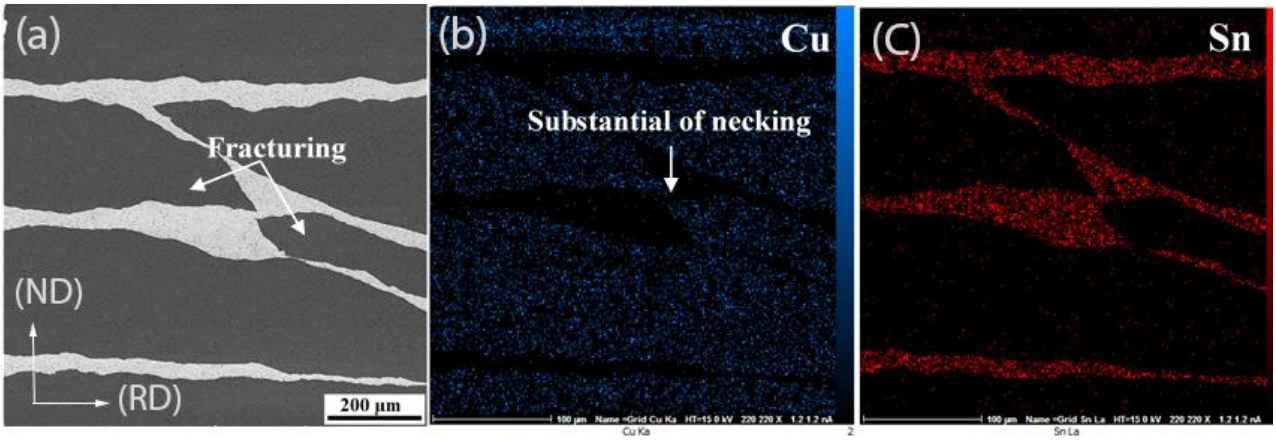

Fig. 3. (a) FESEM image of Cu/Sn composite after three cycles and the corresponding FESEM elemental maps for (b) Cu distribution and (c) Sn distribution.

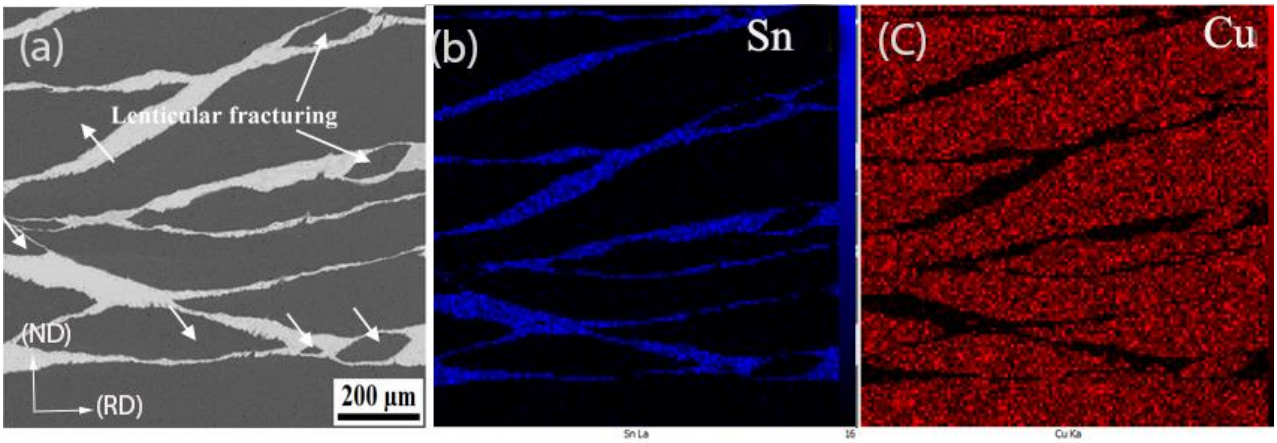

Fig. 4. (a) SEM image of the Cu/Sn composite after four cycles and the corresponding SEM elemental maps for (b) Sn distribution and (c) Cu distribution.

As can be seen, the thinning and necking of the Sn layers are more pronounced. At this stage, the lenticular fragment of copper is simultaneously created in the structure. Another important feature of the co-deformation of the multilayer composites and the final microstructure in the ARB process is the initial thickness ratio and location of the hard and soft layers in the initial sandwich. In the multilayer composite systems, in which initial thickness of the soft layer is more than that of the hard layer a uniform distribution of the hard layer can be observed in the soft layer matrix [26, 36] in the final microstructure. As discussed earlier [18], depending on the hardness ratio, the difference between the flaw properties of the two phases and the thickness of the layers, there are two types of structure, resulting from the co-deformation of the multilayer composites: the wavy structure and lenticular figments of the hard phase in the soft metal matrix. In addition, the relative location of the hard and soft layer affects the microstrucrure [37]. In the multilayer composite systems whose initial thickness of the soft layer is more than that of the hard layer, the hard layer necks and breaks in the early stages. And the final microstructure consists of a uniform distribution of the fragmented hard layer in the soft layer matrix [26, 36]. On the other hand, in the systems with thicker hard phase, the soft layer does not have the ability to deform the hard layer rapidly. Hence, the necking of the hard layer is delayed and the layer continuity remains for further stages given that by increasing the hard layer thickness the strain incompatibility between the layers decreases and the threshold reduction for the occurrence of the necking and fracture in the hard layer increases [37]. In the present research, the thicknesses of the copper and thin layers are 0.9 and 0.5 mm, respectively. In the primary sandwich, one tin layer is in the middle of two layers of copper. Hence, the total thickness of copper is 1.8, that of tin is 0.5 mm, and the hard layer thickness is more than that of the soft layer. Therefore, despite the fact that the metals of this system have a high hardness ratio, as shown in Fig. 5, it is plausible that the final structure in the 7th and 8th cycles is wavy.

By continuing the ARB process more deformation was performed on the samples and in certain areas, making recognizing the Sn and Cu layers more difficult. Fig. 6 reveals a detailed examination of microstructural micrographs with higher magnification from 5 to 8 cycles. The figure reveals certain dark gray areas (the black arrows) inside the Sn layers. To analyze the related areas, the EDS and XRD tests were carried out.

Figure 7 depicts the EDS examination data pertinent to the kind of Sn matrix dark phases in the 6th cycles. The inspection discloses that the dark phases comprise of Cu and Sn. Additionally, the Cu-to-Sn atomic percentage ratio is roughly 1.18.

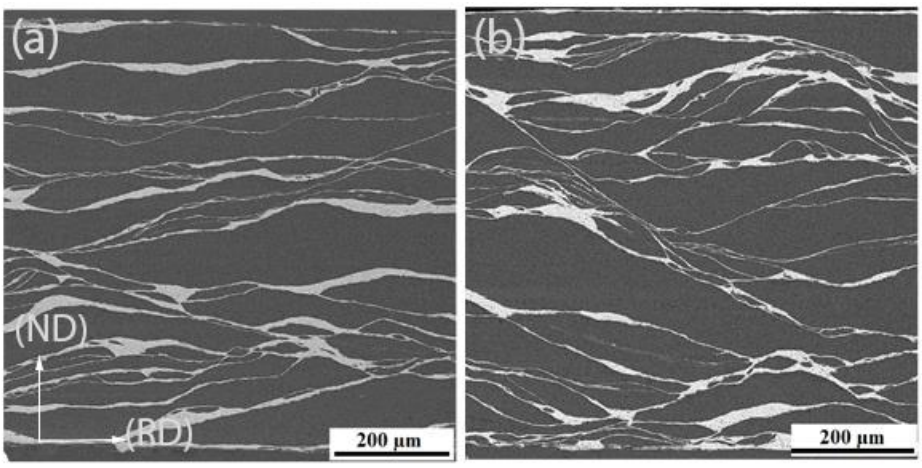

Fig. 5. SEM image of the Cu/Sn composite after a) seven and b) eight cycles.

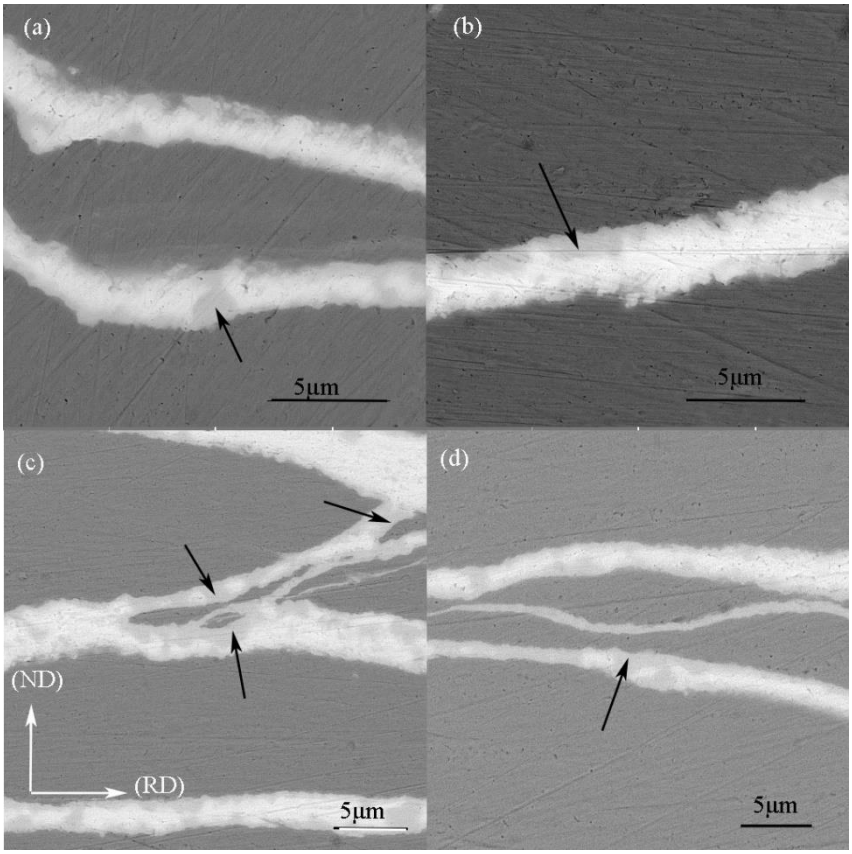

Fig. 6. FESEM micrographs of the ARB-processed Cu/Sn composites with high magnification after: (a) five, (b) six, (c) seven and (d) eight cycles.

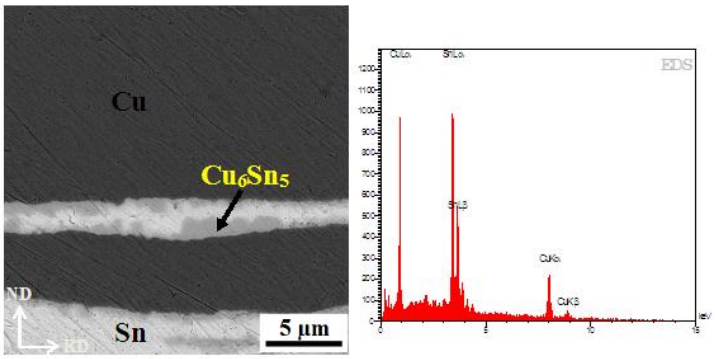

Element	Wt%	At%
Cu	68.83	54.17
Sn	31.17	45.83

Fig. 7. The results of the EDS analysis of dark phases in the Sn matrix in the sixth cycles.

The samples XRD patterns concerning 2, 4, 5, 6 and 8 ARB cycles have been portrayed in Fig. 8. The entire patterns demonstrate reflections on the grounds of the copper elements, and from the 4th cycle onwards, the Sn peaks have been displayed. The Sn peaks intensity is relatively small after 5 cycles. In the initial ARB phases, the surface layer thickness is greater compared to the penetration depth of the x-ray and, therefore, a small amount of Sn could be observed. The Sn peak intensity, especially at low angles rises in the higher cycles of ARB. The important feature of the patterns is that a small peak of Cu_6Sn_5 (η- phase [38]) appears after six cycles. This chemical composition corresponds to the copper and tin ratio obtained from the EDAX analysis.

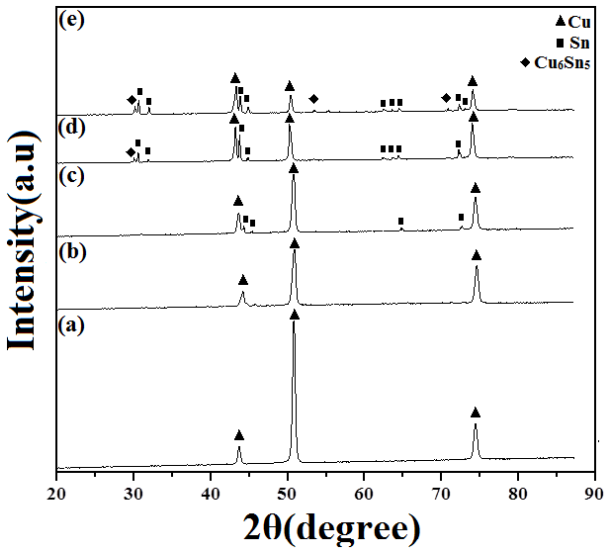

Fig. 8. The XRD patterns for the Cu/Sn composite subjected to (a) two, (b) four, (c) five, (d) six and (e) eight cycles.

As the ARB proceeds and as the layer thickness decreases, the number of interfaces per unit volume rises. Given the 2 μm penetration depth in the typical XRD, there will be a better chance of detecting an interface where intermetallics have been formed. As a result, the intermetallic intensity increases to some degree as the ARB cycles are increased. The formation of intermetallic phases has also been reported during ARB of the other multilayers [16, 17, 23]. The reason can be attributed to the intense straining during ARB, causing an increase in the grain boundaries, the dislocation and the density related to the other defects. In view of the fact that the solid state growth of the Cu_5Sn_6 (η-phase) is attributed to the inter-diffusion of the constituents, namely Cu from the copper layer and Sn from the Sn layer, the formation of boundaries and defects facilitates the elemental diffusion at the interfaces and decreases the activation energy for the formation and solid state growth of the η- phase [16, 38]. As can be seen, no kirkendall porosity and Cu_3Sn (the ε-phase is another Cu-Sn solid state reaction product) were observed. Generally, when Cu and Sn layers are placed in contact with each other under suitable circumstances, the solid state reactions between Cu and Sn produce both Cu_6Sn_5 and Cu_3Sn. The growth of Cu_3Sn tends to induce the formation of Kirkendall voids, while the growth of Cu_6Sn_5 does not [39, 40]. The activation energy (J/mole) for the inter-diffusion in the ε -phase is larger. Therefore, the formation and growth of the ε -layer requires slightly higher temperatures than that of the η-layer [41].

3.2. Mechanical properties

Figures 9 and 10 represent the engineering stress-strain curves of the annealed materials and composites, respectively.

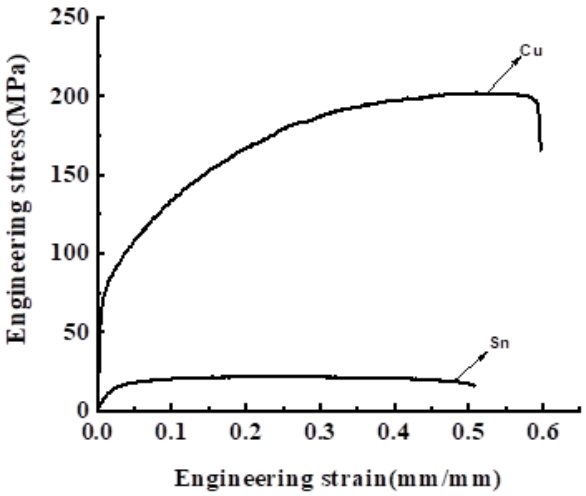

Fig. 9. Engineering stress–strain curves for pure and annealed copper and tin.

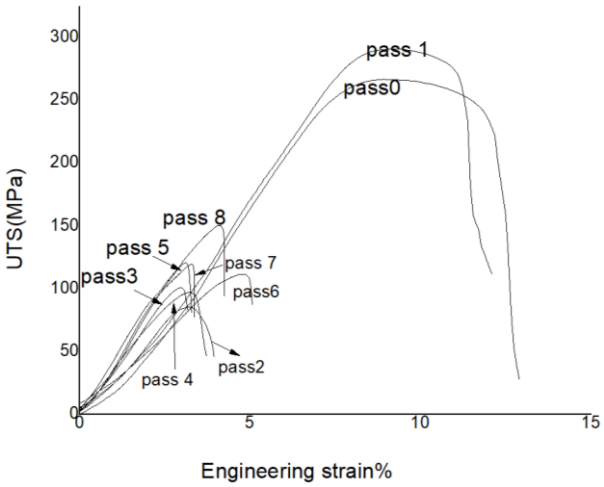

Fig. 10. Engineering stress–strain curves for Cu/Sn composites after different ARB cycles.

The variation in the ultimate tensile stress (UTS) and the percentage elongation with the number of ARB cycles have also been presented in Fig. 11.

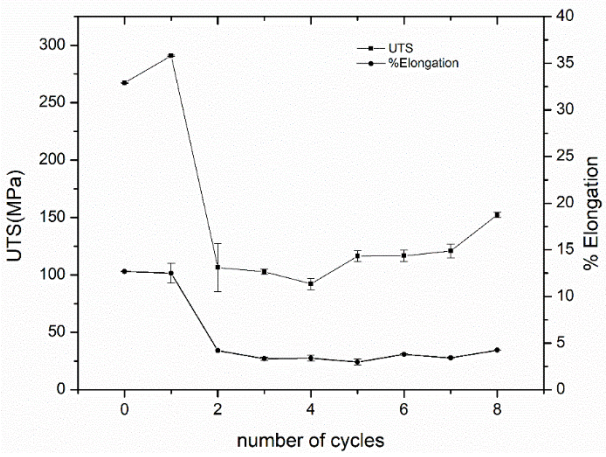

Fig. 11. Variation in UTS and percentage elongation with various ARB cycles.

As can be observed, from zero (the first sandwich sample) to the first cycle, this number increased from well under 275 MPa to just over 292 MPa, which is 1.4 times higher than that of the pure annealed copper. From the first to the second cycle there was a sharp drop in the tensile strength and over the following two cycles it decreased gradually. Afterwards, it increased moderately. Finally, after the eighth cycle the composite exhibited a tensile strength of about 150 MPa, which is 0.72 and 7.7 times the UTS of the pure annealed copper and tin, respectively.

A reduction in the tensile strength has also been reported for the layered composites of Cu/Zn, Al/Sn, Cu/Ni and Mg/Al [16, 18, 26, 42]. As previously stated, the two main mechanisms may contribute to increasing the strength of the produced composites during the ARB cycles: the strain hardening in the early stages and grain refinement in the last stages might be responsible for increasing the strength [20]. Furthermore, the other hardening and softening mechanisms account for the fact that the strength varies with the progress of the ARB cycles. Hardening mechanisms consist of the shear strain, multilayer and dispersion strengthening (because of producing new phases during the process in this case). On the other hand, the necking, rupturing, dynamic recrystallization of the constituents, and creating of micro-cracks and voids in the layers can result in the reduction of strength [16-19].

The hardening mechanisms are explained below:

Shear strain strengthening is the effect of a severe shear deformation precisely below the surface. It has been reported that the severe shear deformation is introduced by the friction between the work piece and the roll under dry conditions. This shear deformation significantly increases the equivalent strain and promotes grain refinement. Moreover, the ARB process can introduce this severely deformed region into the interior of the material by repetition. The whole thickness of materials may be severely strained after several cycles. The other mechanism is the introduction of new interfaces. A large number of interfaces are introduced by several ARB cycles. These interfaces show a well-developed fiber structure [1, 20].

Multilayer Strengthening: As a result of increasing the number of ARB cycles, the thickness of the layers decreases and the number of layers per unit thickness increases. This layer refinement affects the strength of the produced multilayer via the so-called Hall-Petch relationship [20].

Dispersion strengthening in the Cu/Sn System a new intermetallic phase has been created that can help strengthen the composite via dispersion strengthening mechanism.

Increasing the strength from zero to the first cycle of the produced composite can arise from the strain hardening of the layers. The sharp decrease of strength can originate from the softening mechanisms, including the necking of the hard copper phase and the dynamic recrystallization of the Sn layer. The moderate increase of the strength in the last cycles can stem from the grain refinement and the formation of the η- phase.

Figure 11 also implies the variation of the percentage elongation with ARB cycles. It can be observed that the percentage elongation of the multilayer decreases by increasing the ARB cycle. This can be due to the fact that increasing the dislocation density, the strain hardening and an increase in the internal stresses lead to the nucleation of cracks. Besides, the necking and rupturing of the Cu layer are the other reasons for this drop. The formation of Cu_6Sn_5 (η– phase) can be another reason for the elongation decrease in the last cycles.

However, variables like softening mechanisms such as dynamic recovery and dynamic recrystallization, as well as a rise in bonding between the layers interfaces elevate the elongation percentage. In the last steps, the bonding of the layers was raised, softening mechanisms were probably activated, and the intermetallic compounds were developed. Hence, based upon the dominance of the mechanism in each cycle, a rise or a reduction in the elongation percentage takes place [17]. From 1 to 2 cycles the percentage elongation was reduced greatly in view of a drop in dislocations mobility exactly like that in the other severe plastic deformation methods. Then, from 2 to 8 cycles minor fluctuations are witnessed in the percentage elongation, originating from the opposition of augmenting and reducing parameters.

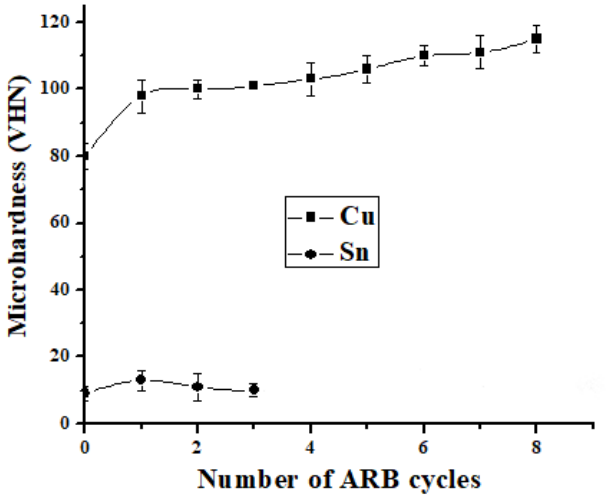

Fig. 12. Variation of microhardness for individual layers with different ARB cycles.

Figure 12 presents data on the amount of hardness for Cu and Sn layers in different ARB cycles. The hardness value of the copper layer increases from well under 80(VHN) to just over 100(VHN) and then it remains constant for the next cycles. Over the following four stages, it rises gradually to approximately 113(VHN). The sharper increase of the hardness value of the copper layer in the first cycle emanates from increasing the dislocation density and formation of sub-grain boundaries, which is a typical trend for hardness during SPD methods [16]. The activation of softening mechanisms like dynamic recovery and recrystallization may contribute to reducing the hardness increase rate. The moderate increase of the hardening rate in the last cycles may come from the grain refinement of the copper layer. The same trend can be seen in the variation of the tin layer hardness value. However, there is a slight fall in the hardness value of the tin layer, resulting from the higher rate of the softening mechanism than that of the hardening mechanism. After the third cycle, the thicknesses of the Sn layers become too small for the researcher to be able to measure the hardness given that the mean diameter of the indented area is larger than the Sn layer thickness. That is why, the microhardness measurement was solely performed up to the third cycle for the Sn layers, yet for the Al layer microhardness, it was measured up to the last cycle. Such a limitation on the micro-hardness of the soft layer in the multilayered composite has also been reported [18].

3.3 Tensile fracture surface

The FESEM image and the corresponding elemental maps of the tensile fracture surfaces of the Cu/Sn multilayer related to the zero cycle of the ARB process have been presented in Fig. 13.

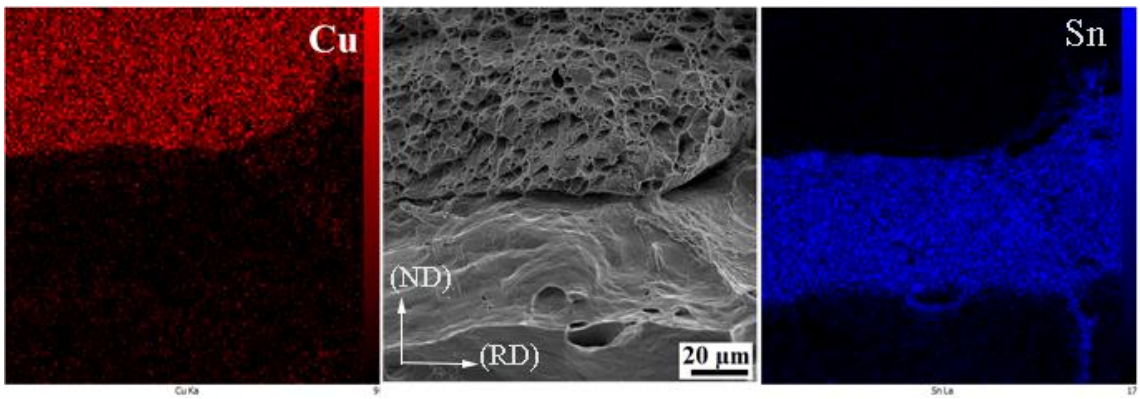

Fig. 13. The FESEM image and the corresponding elemental maps of the tensile fracture surfaces of the Cu/Sn multilayer related to the zero cycle of the ARB process.

At this stage, the fracture appearance of the multilayer reveals the dimples in Cu and Sn layers, indicating that the fracture mode is ductile. Due to the different structures of the two layers, the appearance of the fracture surface is different. The FESEM image of the tensile surface fracture of the produced composites related to the second, fifth and eighth cycles has been presented in Fig. 14. As can be seen, increasing the ARB cycles indicates that the fracture morphology is partially changed after the eighth cycle.

Alternatively, it is axiomatic that a transition from the ductile to the brittle mode is seen in the samples or that the Sn, definitely, undergoes a brittle fracture. After higher ARB cycles (Fig. 14 b, c), it is relatively difficult to identify the individual layers due to an increase in the layer number and a decrease in the layer thickness. The same trend has already been observed in the Al/Sn and Cu/Zn systems [18, 19].

The ductile fracture occurs via the microvoids nucleation and coalescence in advance of the principal crack. Should the second phase particles and inclusions not be present, the void nucleation might commence in view of lack of compatibility of the strain between the two metal components and the slip systems multiplication inside each one of the layers. The number of fracture surface dimples is managed via utilizing the number of nucleated microvoids and the pertinent distribution. Cu, with the FCC structure, has a higher number of slip systems in comparison to Sn with the bct structure. Accordingly, the possibility of the slip systems interconnection (as the microvoids nucleation locations) is higher in Cu than in Sn, which is responsible for the nearer scattering of the dimples inside the Cu layer (Fig.14a) [18].

In other words, it is self-evident that there is a transition from the ductile to the brittle state in certain specimens areas in the samples. After higher ARB cycles (Fig. 14 b, c), it is fairly demanding to specify the single layers on the grounds of a rise in the number of layers and a diminution in their thicknesses. However, obviously, by augmenting the ARB cycles, the dimples depth diminishes and the brittle fractures section is elevated. Such an alteration had previously taken place inside the Al/Sn and Cu/Zn systems [18, 19].

The ductile behavior signifies that the material exhibits the ability to undergo plastic deformation and that in the stress-strain curve there is a considerable distance between the elastic limit and the UTS. As discussed above, the failure behavior becomes more brittle by increasing the ARB steps. Yet as shown in Fig. 10, the ductility of the eighth stage of the produced composite is more than that of the lower ones, such as the fourth stage. This can be a result of increasing the bonding strength between the layers in the final stages, being a result of imposing more deformation and shear strain. Thus, the cracks are less likely to be formed between the layers. Should the strain stress curve of the lower stages be examined closely (like the fourth stage), the distance between the elastic limit and UTS will be found to be greater than that of the final stages. This means that the amount of plastic deformation (uniform elongation) is greater, yet due to the weak layer bonding, the fracture will take place sooner.

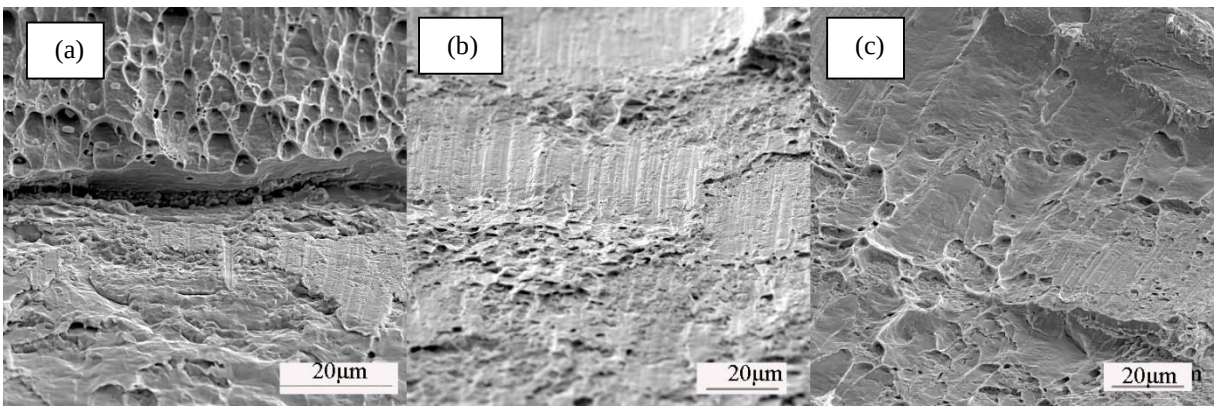

Fig. 14. Tensile fracture surfaces of Cu/Sn composite after (a) one, (b) four and (c) eight cycles.

4. Conclusion

After producing the Cu/Sn multilayer composites, the mechanical and structural properties were evaluated in different ARB cycles and the following conclusions were obtained:

1. Until the initial ARB cycle, the interfaces located between the layers were approximately untouched. After the 2nd cycles, the necked copper layers were cracked in the following cycles. After the 8th ARB cycle, a laminated composite, which possesses the Sn narrow and wavy layers and Cu-distributed lenticular fragments, was obtained.

2. The XRD analysis showed that Cu_6Sn_5 intermetallic (η – phase) has been formed after the sixth ARB cycle and that the amount of this phase increases by increasing the ARB cycles.

3. The maximum tensile strength reached 290 MPa after one ARB cycle, which was around 1.4 and 13 times higher than that of the pure Cu and Sn, respectively; thereafter, it decreased due to the softening mechanism of the Sn layers. Then, it increased moderately and finally after the eighth cycle, the composite exhibited a tensile strength of about 150 MPa, which was 0.72 and 7.7 times the UTS of the pure annealed copper and tin, respectively.

4. By increasing the number of ARB cycles, the ductility of the composites significantly decreased due to strain hardening and reached a plateau in the last cycle.

5. The hardness value of the copper layer increased sharply in the first cycle and, then, it remained constant for the next two cycles and, later rising over the following four stages. The same trend was observed in the variation of the hardness value of the tin layer. However, there was a slight fall in the hardness value of the tin layer, resulting from the higher rate of the softening mechanism than the hardening one.

6. The FESEM micrographs of the fractured surfaces exhibited a ductile fractures mode in the two layers. However, due to the different crystal structure of copper (FCC) and tin (BCT), the number of dimples on the fracture surface of the copper layers was greater and deeper than that of the tin layers.

5. References

[1] Y. Saito, N. Tsuji, H. Utsunomiya, T. Sakai, R.G. Hong, Ultra-fine grained bulk aluminum produced by accumulative roll-bonding proces, *Scripta Materialia*, 40 (1999) 795-800.

[2] M. Delshad Gholami, R. Hashemi, M. Sedighi, M.D. Gholami, R. Hashemi, M. Sedighi, The effect of temperature on the mechanical properties and forming limit diagram of aluminum strips fabricated by accumulative roll bonding process, *Journal of Materials Research and Technology*, 9 (2020) 1831-1846.

[3] S.A. Hosseini, H.D. Manesh, High-strength, high-conductivity ultra-fine grains commercial pure copper produced by ARB process, *Materials and Design*, 30 (2009) 2911-2918.

[4] S. Ghafari-Gousheh, S. Hossein Nedjad, J. Khalil-Allafi, Tensile properties and interfacial bonding of multi-layered, high-purity titanium strips fabricated by ARB process, *Journal of the Mechanical Behavior of Biomedical Materials*, 51 (2015) 147-153.

[5] M. R. Toroghinejad, F. Ashrafizadeh, R. Jamaati, On the use of accumulative roll bonding process to develop nanostructured aluminum alloy 5083, *Materials Science and Engineering A*, 561 (2013) 145-151.

[6] S. Roy, D. Satyaveer Singh, S. Suwas, S. Kumar, K. Chattopadhyay, Microstructure and texture evolution during accumulative roll bonding of aluminium alloy AA5086, *Materials Science & Engineering A*, 528 (2011) 8469-8478.

[7] C. Lei, X. Deng, X. Li, Z. Wang, Simultaneous enhancement of strength and ductility through coordination deformation and multi-stage transformation induced plasticity (TRIP) effect in heterogeneous metastable austenitic steel, *Scripta Materialia*, 162 (2019) 421-425.

[8] X. Rao, Y. Wu, X. Pei, Y. Jing, L. Luo, Y. Liu, J. Lu, Influence of rolling temperature on microstructural evolution and mechanical behavior of AZ31 alloy with accumulative roll bonding, *Materials Science and Engineering: A*, 754 (2019) 112-120.

[9] X. Luo, Z. Feng, T. Yu, T. Huang, R. Li, G. Wu, N. Hansen, X. Huang, Microstructural evolution in Mg-3Gd during accumulative roll-bonding, *Materials Science and Engineering A*, 772 (2020) 138763.

[10] X.Y. Yang, Q.S. Mei, X.M. Mei, Y. Ma, F. Chen, L. Wan, J.Y. Li, Materials Science & Engineering A Al matrix composites reinforced by high volume fraction of TiAl 3 fabricated through combined accumulative roll-bonding processes, 754 (2019) 309-317.

[11] F. Ferreira, I. Ferreira, E. Camacho, F. Lopes, A.C. Marques, A. Velhinho, Graphene oxide-reinforced aluminium-matrix nanostructured composites fabricated by accumulative roll bonding, *Composites Part B: Engineering*, 164 (2019) 265-271.

[12] A. Melaibari, A. Fathy, M. Mansouri, M.A. Eltaher, Experimental and numerical investigation on strengthening mechanisms of nanostructured Al-SiC composites, *Journal of Alloys and Compounds*, 774 (2019) 1123-1132.

[13] S. Mansourzadeh, M. Hosseini, E. Salahinejad, A.H. Yaghtin, Cu-(B4C)p metal matrix composites processed by accumulative roll-bonding, *Progress in Natural Science: Materials International*, 26 (2016) 613-620.

[14] G.P.P. Zhang, Q.S.S. Mei, C.L.L. Li, F. Chen, X.M.M. Mei, J.Y.Y. Li, X.F.F. Ruan, Fabrication and properties of Al-TiAl3-Al2O3 composites with high content of reinforcing particles by accumulative roll-bonding and spark plasma sintering, *Materials Today Communications*, 24 (2020) 3-8.

[15] A.I. Khadir, A. Fathy, A.I. Khdair, A. Fathy, Enhanced strength and ductility of Al-SiC nanocomposites synthesized by accumulative roll bonding, *Journal of Materials Research and Technology*, 9 (2020) 478-489.

[16] L. Ghalandari, M.M. Mahdavian, M. Reihanian, Microstructure evolution and mechanical properties of Cu/Zn multilayer processed by accumulative roll bonding (ARB), *Materials Science and Engineering A*, 593 (2014) 145-152.

[17] M.M.M. Mahdavian, L. Ghalandari, M. Reihanian, Accumulative roll bonding of multilayered Cu/Zn/Al: An evaluation of microstructure and mechanical properties, *Materials Science and Engineering A*, 579 (2013) 99-107.

[18] L. Ghalandari, M.M.M. Mahdavian, M. Reihanian, M. Mahmoudiniya, Production of Al/Sn multilayer composite by accumulative roll bonding (ARB): A study of microstructure and mechanical properties, *Materials Science and Engineering A*, 661 (2016) 179-186.

[19] A. Mashhadi, A. Atrian, L. Ghalandari, Mechanical and microstructural investigation of Zn/Sn multilayered composites fabricated by accumulative roll bonding (ARB) process, *Journal of Alloys and Compounds*, 727 (2017) 1314-1323.

[20] L. Ghalandari, M.M. Moshksar, High-strength and high-conductive Cu/Ag multilayer produced by ARB, *Journal of Alloys and Compounds*, 506 (2010) 172–178.

[21] D.C.C. Magalhães, V.L. Sordi, A.M. Kliauga, Microstructure evolution of multilayered composite sheets of AA1050/AA7050 Al alloys produced by Asymmetric Accumulative Roll-Bonding, *Materials Characterization*, 162 (2020) 110226.

[22] L.F. Zhang, R. Gao, B.L. Zhao, M. Sun, K. Jing, X.P. Wang, T. Hao, Z.M. Xie, R. Liu, Q.F. Fang, C.S. Liu, Effects of annealing temperature and layer thickness on hardening behavior in cross accumulative roll bonded Cu/Fe nanolamellar composite, *Journal of Alloys and Compounds*, 827 (2020) 154312.

[23] M.M. Mahdavian, H. Khatami-Hamedani, H.R. Abedi, Macrostructure evolution and mechanical properties of accumulative roll bonded Al/Cu/Sn multilayer composite, *Journal of Alloys and Compounds*, 703 (2017) 605-613.

[24] M. Talebian, M. Alizadeh, Manufacturing Al/steel multilayered composite by accumulative roll bonding and the effects of subsequent annealing on the microstructural and mechanical characteristics, *Materials Science and Engineering A*, 590 (2014) 186-193.

[25] R.N. Dehsorkhi, F. Qods, M. Tajally, Investigation on microstructure and mechanical properties of Al-Zn composite during accumulative roll bonding (ARB) process, *Materials Science and Engineering A*, 530 (2011) 63-72.

[26] M. Tayyebi, B. Eghbali, Study on the microstructure and mechanical properties of multilayer Cu/Ni composite processed by accumulative roll bonding, *Materials Science and Engineering A*, 559 (2013) 759-764.

[27] M. Alizadeh, M. Talebian, Fabrication of Al/Cu p composite by accumulative roll bonding process and investigation of mechanical properties, *Materials Science and Engineering A*, 558 (2012) 331-337.

[28] C. Hai, Z. Mingyi, Effect of Intermetallic Compounds on the Fracture Behavior of Mg/Al Laminated Composite Fabricated by Accumulative Roll Bonding, *Rare Metal Materials and Engineering*, 45 (2016) 2242-2245.

[29] M. Alizadeh, M. Samiei, Fabrication of nanostructured Al/Cu/Mn metallic multilayer composites by accumulative roll bonding process and investigation of their mechanical properties, *Materials and Design*, 56 (2014) 680-684.

[30] G. Anne, M.R. Ramesh, H.S. Nayaka, S.B. Arya, Investigation of microstructure and mechanical properties of Mg–Zn/Al multilayered composite developed by accumulative roll bonding, *Perspectives in Science*, 8 (2016) 104-106.

[31] S. Roy, B.R. Nataraj, S. Suwas, S. Kumar, K. Chattopadhyay, Accumulative roll bonding of aluminum alloys 2219/5086 laminates: Microstructural evolution and tensile properties, *Materials and Design*, 36 (2012) 529-539.

[32] K. Wu, H. Chang, E. Maawad, W.M. Gan, H.G. Brokmeier, M.Y. Zheng, Microstructure and mechanical properties of the Mg/Al laminated composite fabricated by accumulative roll bonding (ARB), *Materials Science and Engineering: A*, 527 (2010) 3073-3078.

[33] F. Emitters, Supramolecular Chemistry of Fullerenes and Carbon Nanotubes Carbon Nanotube and Related Raman Spectroscopy in Graphene Related Systems Carbon Materials and Nanotechnology Carbon Nanomaterials Carbon Nanotubes and Related Structures.

[34] H.M. Mallikurjuna, K.T. Kashyap, P.G. Koppad, C.S. Ramesh, R. Keshavamurty, Microstructure and dry sliding wear behavior of Cu-Sn alloy reinforced with multiwalled carbon nanotubes, *Transactions of Nonferrous Metals Society of China (English Edition)*, 26 (2016) 1755-1764.

[35] O. Yılmaz, H. Turhan, The relationships between wear behavior and thermal conductivity of CuSn / M7 C3 – M 23 C 6 composites at ambient and elevated temperatures, *Composites Science and Technology*, 61 (2001) 2349-2359.

[36] Y.M. Hwang, H.H. Hsu, H.J. Lee, Analysis of plastic instability during sandwich sheet rolling, *International Journal of Machine Tools and Manufacture*, 36 (1996) 47-62.

[37] M. Rahdari, M. Reihanian, S.M.L. Baghal, Microstructural control and layer continuity in deformation bonding of metallic laminated composites, *Materials Science and Engineering A*, 738 (2018) 98-110.

[38] A.C.K. So, Y.C. Chan, J.K.L. Lai, Aging studies of Cu-Sn intermetallic compounds in annealed surface mount solder joints, *IEEE Transactions on Components Packaging and Manufacturing Technology Part B*, 20 (1997) 161–166.

[39] Y. Shu, S. Gheybi, T. Ando, Z. Gu, Ultrasonic powder consolidation of Sn/In nanosolder particles and their application to low temperature Cu-Cu joining, *JMADE*, 111 (2016) 631-639.

[40] Y.W. Wang, Y.W. Lin, C.R. Kao, Kirkendall voids formation in the reaction between Ni-doped SnAg lead-free solders and different Cu substrates, *Microelectronics Reliability*, 49 (2009) 248-252.

[41] T. Laurila, V. Vuorinen, J.K. Kivilahti, Interfacial reactions between lead-free solders and common base materials, *Materials Science and Engineering R: Reports*, 49 (2005) 1-60.

[42] M.C. Chen, H.C. Hsieh, W. Wu, The evolution of microstructures and mechanical properties during accumulative roll bonding of Al/Mg composite, *Journal of Alloys and Compounds*, 416 (2006) 169-172.